ACS Biomaterials SCIENCE & ENGINEERING

pubs.acs.org/journal/abseba

Article

Elastin-like Proteins to Support Peripheral Nerve Regeneration in Guidance Conduits

Riley A. Suhar, Laura M. Marquardt, Shang Song, Hana Buabbas, Vanessa M. Doulames, Patrik K. Johansson, Katarina C. Klett, Ruby E. Dewi, Annika M. K. Enejder, Giles W. Plant, Paul M. George, and Sarah C. Heilshorn*

Cite This: *ACS Biomater. Sci. Eng.* 2021, 7, 4209–4220

Read Online

ACCESS | Metrics & More | Article Recommendations | Supporting Information

ABSTRACT: Synthetic nerve guidance conduits (NGCs) offer an alternative to harvested nerve grafts for treating peripheral nerve injury (PNI). NGCs have been made from both naturally derived and synthesized materials. While naturally derived materials typically have an increased capacity for bioactivity, synthesized materials have better material control, including tunability and reproducibility. Protein engineering is an alternative strategy that can bridge the benefits of these two classes of materials by designing cell-responsive materials that are also systematically tunable and consistent. Here, we tested a recombinantly derived elastin-like protein (ELP) hydrogel as an intraluminal filler in a rat sciatic nerve injury model. We demonstrated that ELPs enhance the probability of forming a tissue bridge between the proximal and distal nerve stumps compared to an empty silicone conduit across the length of a 10 mm nerve gap. These tissue bridges have evidence of myelinated axons, and electrophysiology demonstrated that regenerated axons innervated distal muscle groups. Animals implanted with an ELP-filled conduit had statistically higher functional control at 6 weeks than those that had received an empty silicone conduit, as evaluated by the sciatic functional index. Taken together, our data support the conclusion that ELPs support peripheral nerve regeneration in acute complete transection injuries when used as an intraluminal filler. These results support the further study of protein engineered recombinant ELP hydrogels as a reproducible, off-the-shelf alternative for regeneration of peripheral nerves.

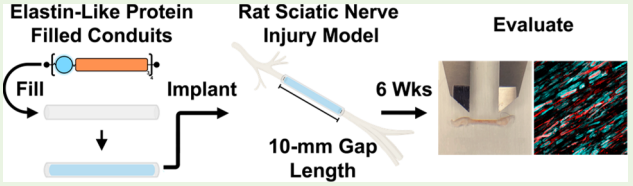

KEYWORDS: *Nerve guidance conduit, peripheral nerve, protein engineering, elastin-like protein*

INTRODUCTION

Peripheral nerve injury (PNI) results from acute or chronic damage to the peripheral nervous system (PNS), which can lead to a permanent loss of motor or sensory function.[1] Many incidents of PNI require surgical intervention, and although advances in microsurgical techniques to repair nerves have improved patient outcomes[2] satisfactory results are still severely lacking. For example, one meta-analysis looking at surgical cases for repairing complete transections of the median and ulnar nerves found that as few as 51.6% of patients (n = 281 cases) achieved satisfactory motor function and 42.6% of patients (n = 380 cases) achieved satisfactory sensory function.[3] PNI is most prevalent in upper extremities such as the ulnar nerve, which controls lower arm and hand function, resulting in significant loss of function. As these injuries disproportionately affect younger populations, PNI often represents a life-long impact on quality of life.[4] Thus, PNI is an area in need of improved therapeutic intervention.

The current clinical "gold standard" for treating PNI is the nerve autograft.[5] Autografts have significant drawbacks including donor site tissue morbidity, limited donor tissue supply, and the associated risk and cost of a second surgery.[6,7] Given these limitations, there has been an effort to move to alternative therapeutics. Nerve allografts from cadaveric donors avoid injury to the host, but challenges include limited cadaveric tissue supply and host-rejection requiring immunosuppression.[8] Recent advances in decellularization methods have made acellular nerve grafts a promising clinical alternative.[9] However, these harvested tissues still require cadaveric donors in addition to costly isolation and preparation. An off-the-shelf, fully synthetic nerve guidance conduit (NGC) would be beneficial to the field.

The conventional design for a synthetic NGC is a hollow cylinder that directly bridges the proximal and distal nerve stumps following microsurgical implantation. It is well documented that hollow NGCs lead to poor neural regeneration, as the absence of a support matrix for regenerating nerves drastically reduces the potential for extending neurites to reach their distal targets.[10,11] To alleviate this, numerous materials have been used to fill the intraluminal

Special Issue: Advanced Biomedical Hydrogels

Received: July 15, 2020
Accepted: October 20, 2020
Published: November 4, 2020

https://dx.doi.org/10.1021/acsbiomaterials.0c01053
ACS Biomater. Sci. Eng. 2021, 7, 4209–4220

space to provide this necessary support. Examples of filler materials can be divided into two broad categories: (1) naturally derived materials and (2) synthesized materials. Naturally derived materials like collagen, fibrin, keratin, laminin, and decellularized sciatic-nerve-based gels have been used as luminal fillers and have been shown to promote neurite regeneration.[12−17] However, by virtue of being naturally derived, they are hard to control systematically and have inherent batch-to-batch variability. Alternatively, synthesized intraluminal materials like poly(lactic-*co*-glycolic acid) (PLGA), polyurethanes, and polycaprolactone (PCL) present excellent tunability and reproducibility compared to naturally derived materials; however, they lack biochemical cues and require the addition of extracellular matrix (ECM) materials or secondary chemical modifications to make them bioactive.[18−22] In short, while naturally derived materials typically offer better bioactivity, synthetic materials offer increased material control and reliability.

Recombinant protein engineering is a strategy that can merge the benefits of these two classic material sources for the treatment of PNI. Protein engineering allows for the highly controlled design of polypeptides by leveraging recombinant DNA to precisely define protein sequences.[23,24] Through careful design of these DNA sequences, the resulting protein can be tailored to contain a number of biochemical cues similar to those found in native ECM materials and tuned to exhibit a spectrum of mechanical properties.[25] Recombinant elastins in particular are potentially useful for biomedical applications given their high relative stability, making them suitable for long-term storage, particularly in sterile environments. Elastins have a high hydrophobicity and resistance to degradation outside of a select few matrix metalloproteinases, with some studies estimating a half-life as long as 40 years.[26−28]

Using this technique, we previously reported the design of a family of elastin-like proteins (ELPs) that have independently tunable matrix mechanics and cell-adhesive properties.[29−31] Hydrogels composed of covalently cross-linked ELPs can be tailored to regulate neural progenitor cell stemness[32] and neurite outgrowth from isolated chick dorsal root ganglia (DRG) cultures *in vitro*.[33] Although ELPs have been used as an injectable drug depot to treat neuroinflammation in the PNS,[34] they have not been used as a support matrix for regenerating axons in treating PNI. Given the need for innovative, synthetic materials for NGCs, the present study aimed to assess if ELP hydrogels can be used to support nerve outgrowth *in vivo*. To address this question, we employed the commonly used sciatic nerve transection injury model, which is the most accepted small animal model for assessing PNI therapeutics.[35] Two conduit types, an ELP-filled silicone conduit and an empty silicone conduit, were implanted at the site of a 10 mm sciatic nerve injury gap in the main nerve trunk (proximal to the trifurcation) following acute transection in rats. Over the course of 6 weeks, animals in each group were assessed for functional recovery using the sciatic functional index (SFI). Post euthanasia, innervation quality and extent of regeneration were assessed using electrophysiological measurements, gross histology, and immunohistochemistry.

MATERIALS AND METHODS

Elastin-like Protein Expression. ELPs were expressed in BL21 (DE3) pLysS *Escherichia coli* (Invitrogen, 1931008) under control of the T7 promoter, as previously described.[29] Briefly, *E. coli* was grown in Terrific Broth (Fisher, BP9728-5) at 37 °C to an optical density (λ = 600 nm) of 0.8, and expression was induced by addition of 1 mM isopropyl β-d-1-thiogalactopyranoside (IPTG; Thermo, BP1755-100). After 7 h of expression, cells are collected by centrifugation, resuspended in TEN buffer (0.1 M Tris-Cl, 0.01 M EDTA, 1 M NaCl, pH 8.0) at 25 g cells per 100 mL, and then frozen at −80 °C overnight. To release expressed proteins, the cell membrane is disrupted via repeated freeze−thaw cycles (three total cycles; freezing at −80 °C, thawing at 4 °C). 1 mM phenylmethylsulfonyl fluoride ((PMSF); ThermoScientific) and ∼30 mg of deoxyribonuclease I (Sigma) are added after the first cycle to prevent protease activity and to degrade DNA, respectively. ELPs are purified from cell components by thermal cycling and leveraging the lower critical solution temperature (LCST) behavior, which is induced at ∼33 °C for our ELPs.[29] In this procedure, the solution is first cooled to 4 °C and then centrifuged at ≥15 000×*g* at 4 °C, and the resulting supernatant containing solubilized ELP is collected. This solution is then incubated at 37 °C, which induces the LCST behavior and forms a two-phase mixture of ELP and solution. Precipitation is further assisted by the addition 0.1 M NaCl. The resulting two-component mixture is centrifuged at ≥15,000×*g*, 37 °C, and the ELP-containing pellet is then solubilized in fresh water and cooled overnight under constant agitation at 4 °C. This thermal cycling procedure is repeated a total of three times. To remove the exogenously added salt, the resulting solution is dialyzed against 4 L of ultrapure deionized water at 4 °C with constant rotation. The 4 L of dialysis water is routinely refreshed every 12 h over the course of 3 days. The final dialyzed product is then sterilized using a 0.22 μm syringe filter, frozen, and finally lyophilized for 3 days. The final lyophilized product is stored in a sterile 50 mL tube at 4 °C in the presence of desiccant to prevent water accumulation.

Hydrogel Formation. To fabricate our hydrogels, ELP was dissolved (3.75% (w/v) in Dulbecco's phosphate-buffered saline (DPBS)) in a 1.5 mL tube overnight at 4 °C on a constant rotator. The following day, the ELP solution was placed on ice and cooled for at least 15 min. For cross-linking, we selected the amine-reactive cross-linker tetrakis(hydroxymethyl)phosphonium chloride (THPC; Sigma). THPC was dissolved (2.7 μL THPC/1 mL DPBS) in a 1.5 mL tube, homogenized by manual inversion and then cooled on ice for approximately 10 min. To reach a final ELP concentration of 3% (w/v) ([RGD] = 3.1 mM) and cross-link 100% of the available lysine groups, we combined the ELP and THPC solutions in a 4:1 ratio and thoroughly mixed them by vigorous pipetting while taking care to avoid any bubble formation but ensure complete mixing. This formulation and fabrication procedure is used for all hydrogels in the present work. Additionally, for ease of viewing purposes ELP-hydrogels can be dyed blue using any standard food coloring additive. In the present manuscript, blue-colored ELP hydrogels were prepared for visualization by supplementing the THPC solution with 1 μL of blue food coloring (Market Pantry) prior to mixing with ELP.

Hydrogel Mechanical Characterization. Shear-rheology was carried out on a stress-controlled ARG2 rheometer (TA Instruments) using a 20 mm diameter, cone-on-plate geometry. All tests were conducted on 50 μL samples with a humidity chamber to prevent dehydration over the course of the experiment. To demonstrate hydrogel formation, a time-sweep was performed at 23 °C with an oscillatory strain of 1% at an angular frequency of 1 rad/s over the course of 30 min. Evidence of gel-formation was indicated by the crossover point, where the storage modulus (G') was greater than the loss modulus (G''). For the reported stiffness measurements, hydrogel samples were cross-linked at 23 °C for 30 min. The temperature was then ramped to 37 °C at a ramp rate of 3 °C/min and incubated for 15 min at 37 °C to ensure complete cross-linking and to allow for any stiffening effects from thermal aggregation of the ELP. After incubation, samples were exposed to an amplitude sweep (1−300% strain, 1 rad/s angular frequency), and G' was reported from within the linear-elastic regime before the onset of any yielding behavior. For consistency, the G' reported in the present study was reported for 10% strain. In the present experiment, four independent samples were measured and averaged as a representative matrix stiffness.

https://dx.doi.org/10.1021/acsbiomaterials.0c01053
ACS Biomater. Sci. Eng. 2021, 7, 4209−4220

Conduit Fabrication. The outer shells of our conduits were made from silicone tubing (VWR, 32829-170) with cross-sectional dimensions of 0.078 in (1.9812 mm) and 0.125 in (3.175 mm) for the inner and outer diameters, respectively. To make each conduit, tubing was cut into 14 mm long sections and then sterilized by immersion in 70% ethanol for 72 h. Conduit shells were then air-dried in a tissue culture hood to maintain sterility. To designate the implant gap length, conduits were lightly marked with an ethanol-resistant marker (Fisher) 2 mm from either end of the conduit. Conduits that were to be implanted with no support matrix (empty silicone conduits) were then transferred to autoclaved 1.5 mm microfuge tubes and submerged in sterile saline solution. For the ELP-filled conduits, predissolved, prechilled ELP and THPC solutions were mixed as described previously (total solution volume of 23 μL per conduit) and then immediately transferred to the sterile silicone conduits via a protein-transfer tip. To avoid any leakage or evaporation, ELP-filled conduits were sealed by clipping each end with a sterilized binder clip and then allowed to cross-link at room temperature for 30 min. Next, the binder clips were removed, and the ELP-filled conduits were gently transferred to autoclaved 1.5 mL tubes filled with prewarmed 37 °C saline solution. To ensure complete cross-linking, tubes containing ELP-filled conduits were further incubated in a 37 °C bath for 15 min prior to storage. All implants were made the night before surgery.

Sciatic Nerve Surgery and Animal Euthanasia. This protocol was approved by the Stanford Administrative Panel on Laboratory Animal Care. The National Institutes of Health (NIH) guidelines for the care and use of laboratory animals were observed (NIH publication no. 85-23 Rev. 1985). All animals were purchased from Charles River and caged in gender-matched pairs for the duration of this protocol. Food and water were administered ad libitum, and their environment was temperature and humidity controlled with a 12 h on, 12 h off light schedule. Animals were checked every other day over the course of the experiment for any signs of stress or injury to ensure a safe environment.

The sciatic nerve injury model was carried out in accordance with established methods described in the literature.[35] Mixed-gender Sprague−Dawley rats (10 week old, n = 25) were anesthetized using 1−3% isoflurane mixed with 1% oxygen. The right hind leg was then gently shaved using animal hair clippers, and the area was wiped clean first with Betadine solution and then three times successively with 70% ethanol solution using a sterile gauze strip. After making a parallel incision on top of the femur and separating the skin from the underlying muscles, the sciatic nerve was exposed through a dorsal/gluteal splitting via blunt dissection with sterilized surgical scissors. The sciatic nerve was then carefully separated from the surrounding muscle by removal of connective tissue along the length of the operating area to clearly expose the main trunk of the nerve and distal trifurcation. Once exposed and cleared, the sciatic nerve was fully transected approximately 2 mm above the trifurcation, and a 5 mm section of the proximal nerve was removed using heat-sterilized microscissors under a microscope. Conduits were trimmed such that there was ∼1 mm overhang on either end of the predesignated 10 mm gap. The proximal and distal stumps of the sciatic nerve were then secured into the conduits with two 9-0 nylon (Ethicon) sutures per end. After securing the nerve guidance conduit, the previously dissected muscles were sutured together with 4-0 nylon sutures (Ethicon), and the fold between the dissected skin and overlaying muscle was gently cleaned with sterile saline solution to remove any residual blood. The skin was then closed by careful suturing with 4-0 nylon sutures, and the surgical area then was wiped clean of any residual blood or fur. The animal was left to wake up under the presence of 1% oxygen before being returned to their cage.

Immediately following surgery, animals were given subcutaneous (SQ) injections of buprenorphine SR (1.2 mg/kg) and penicillin G (100 000 units/animal). For the 3 days following surgery, animals were given additional SQ injections of penicillin G twice daily to prevent any postoperative infection. For the first week, animals were checked daily for signs of stress or postoperative complications. From the second week to the conclusion of the experiment, animals were checked every other day for signs of stress or injury. At the conclusion of the experiment, animals were anesthetized with 1−3% isoflurane and 1% oxygen. While anesthetized, animals were euthanized via intracardiac injection of sodium pentobarbital euthanasia solution (200 mg/kg) using a 27G needle.

Sciatic Functional Index Measurements. To measure the sciatic functional index (SFI), we first constructed a clear-bottom plastic box (24″ x 24″ x 24″) to create a confined space that was large enough to allow for free movement for the animals. The clear box was suspended above a high definition Webcam (Logitech, C922 Pro Stream) and animals were recorded walking for a total of 10 min without interference at weekly time points. From this 10 min video, 5 randomly selected still screenshots were taken in which both hind paws were clearly visible and resting in the plantar position (all toes clearly visible). To further ensure that the selected images were representative of their toe spread, all stills came from individual full gaits (all paws run through a full cycle of walking) and any stills in which the animal was standing (resting on hind paws only) were excluded. From the individual stills, the (1) paw length (PL; length between tip of center toe to furthest point of contact on back of foot), (2) toe spread (TS; length between first to fifth digit), and (3) intermediary toe spread (IT; length between the second and fourth digit) were measured for both the uninjured (N; "normal") and injured (E; "experimental") sides. These values were then utilized to calculate the commonly used Bain-Mackinnon-Hunter SFI using the following equation first reported in Bain et al.[36]

$$\mathrm{SFI} = -38.3 \times \left(\frac{\mathrm{EPL} - \mathrm{NPL}}{\mathrm{NPL}}\right) + 109.5\left(\frac{\mathrm{ETS} - \mathrm{NTS}}{\mathrm{NTS}}\right) + 13.3\left(\frac{\mathrm{EIT} - \mathrm{NIT}}{\mathrm{NIT}}\right) - 8.8 \quad (1)$$

The SFI was calculated from each still image, and these five measurements were averaged together as a representative measurement for each animal at that time point.

All lengths were measured as pixels in Fiji (ImageJ open source software) with the line tool and measurement function, and final SFI was calculated in Excel (Microsoft).[37] All animals were pretrained in this experiment twice a week for 2 weeks prior to surgery. After surgery, each animal was measured weekly (+1, +2, +3, + 4, +5, and +6 week time points). Any animal that had evidence of distress or injury ("autotomy", or toe-biting on the experimental side, is common with this injury model[38−40]) was immediately excluded from additional measurements. In the present work, due to autotomy, four animals had been dropped from the empty silicone conduit group and one animal from the ELP-filled conduit group by the conclusion of the study. All measurements were taken, measured, and quantified by a trained observer blinded to the conditions to reduce testing bias.

Electrophysiology Measurements. Electrophysiology measurements were carried out in accordance with established methods described in the literature.[41−44] Briefly, following euthanasia, previously implanted conduits were exposed through dorsal/gluteal splitting via blunt dissection with sterilized surgical scissors. Any occlusions and connective tissue around the length of the conduits were carefully dissected and removed with microsurgical tools. For probing, an additional 5 mm of uninjured nerve on the proximal side of the conduit was exposed. Any connective tissue was removed to allow for easy isolation and separation from the underlying muscle of the sciatic nerve. Once isolated, a stimulating electrode (length of 12.7 mm, diameter of 0.3 mm; BD Precision) was placed approximately 3 mm proximal of the implant and connected to an external stimulator (Keysight). A corresponding electrode was placed in the ventral side of the experimental (hind right) paw for detecting any resulting compound muscle action potentials (CMAP). The amplifier gain was set to 1000 with a bandpass filter of 300 Hz to 10 kHz. All measurements were recorded with the leg in a relaxed, unobstructed position to avoid possible interference of measured signals from undue contraction/deformation of the sciatic nerve and implanted conduit. Once set up, the stimulating electrode delivered pulses with an intensity from 0 to 1 V at 1 s intervals to repetitively stimulate the

https://dx.doi.org/10.1021/acsbiomaterials.0c01053
ACS Biomater. Sci. Eng. 2021, 7, 4209−4220

sciatic nerve and elicit CMAP responses, which were recorded in the Labchart software package (Powerlab, AD Instrument). After all measurements were taken, the distance between the two electrodes was measured with a stainless-steel ruler and documented for each animal.

From these recordings, the amplitude and conduction were calculated based on a previously published method.[44] To determine the amplitude, we measured the difference between the first positive peak and the baseline, defined as the voltage prior to the stimulating peak. To record the conduction velocity, the distance between the stimulating and measuring electrodes was divided by the latency between the stimulating peak and the time corresponding to the maximum of the first positive peak. For each individual data point, three distinct CMAP signals were randomly selected, and the resulting amplitudes and conduction velocities were averaged.

Sciatic Nerve Tissue Dissection and Fixation. Following removal of connective tissue from implanted conduits and exposure of proximal and distal portions of healthy nerve, a small square window was carefully cut into the outer silicone wall to allow fixative to enter post-transection. The conduits, along with an additional ∼5 mm uninjured nerve on either end, were then carefully dissected from the animal, and a single 9-0 suture was used to mark the proximal end of the nerve. The length of the excised tissue and conduit were placed on a wooden dowel to ensure the tissue fixed in a straight, unobstructed way for easy sectioning. Once adhered to the wooden dowel, any free space in the conduit was filled with 10% buffered formalin and then the dowel and tissue were fully submerged in 10 mL of 10% buffered formalin in a 15 mL tube. Tissues were fixed for 72 h at 4 °C. After fixation, the silicone tubing was carefully removed, and any remaining tissue on the inside of the conduit was bound to a wooden dowel by gentle knotting with a single 4-0 suture to ensure the tissue sample remained in the straight, unobstructed position. Tissues were stored at room temperature in 70% ethanol until paraffin embedding and tissue sectioning. For comparison, 15 mm lengths of the contralateral nerves were removed, fixed, and stored using the same procedure outlined above.

Antigen Retrieval and Immunohistochemistry. Sciatic nerve tissue samples were embedded in paraffin using a step-dehydration protocol. First, tissues were dehydrated through successive 70% and 95% ethanol changes (40 min each) followed by three changes of 100% ethanol (40 min each). Then, the tissue was cleared through three changes of fresh xylene (40 min each). Finally, the dehydrated tissue was immersed in three changes of paraffin (40 min each) and embedded in a paraffin block. Embedded tissues were stored at room temperature until cutting. Tissue blocks were sectioned horizontally (length-wise) into 5 μm thick sections and affixed to histologic slides. Antigen retrieval was performed using a common citrate buffer antigen retrieval protocol as published elsewhere.[45,46] Briefly, slides were deparaffinized in two changes of fresh xylene for 5 min each. Slides were then hydrated stepwise through two changes of 100% ethanol (3 min), one change of 95% ethanol (1 min), one change of 70% ethanol (1 min), and then gently submerged in room temperature water. Slides were then immersed in a staining dish filled with sodium citrate buffer (2.94 g of trisodium citrate dihydrate and 0.5 mL of Tween 20 in 1 L of water, pH 6.0, sterile filtered) and incubated for 40 min at 95 °C. Tissue sections were then cooled in the sodium citrate buffer for 20 min to room temperature and then immersed in two fresh changes of DPBS with 0.05% Tween 20 for 2 min.

After antigen retrieval, excess solution around the edges and back of each slide was removed by careful drying with a clean paper towel, and the edges were filled in with a hydrophobic pen (Fisher) to limit the amount of antibody solution necessary. Tissues were blocked with 250 μL of blocking solution (0.1% Triton X-100, 10% goat serum in DPBS) for 4 h at room temperature. Blocked slides were then stained with primary antibodies in Triton X-100 PBS solution (0.1% Triton X-100 in DPBS; antineurofilament, Abcam, ab1987, 1:200 dilution and antimyelin basic protein, Abcam, ab7349; 1:400 dilution) for 72 h at 4 °C in a sealed histology container with ∼0.5 cm of water to prevent dehydration. Tissue slides were then washed four times for a total of 20 min with Triton X-100 solution. Washed tissue sections were then stained with 250 μL of secondary antibodies in Triton X-100 solution (antirabbit AF488, Abcam, ab150077, 1:400 and antirat AF546, Invitrogen, A-11081, 1:400) for 24 h at 4 °C. Tissue sections were then washed three times for 20 min each with Triton X-100 DPBS solution. Finally, stained slides were mounted with a coverslip using ProLong Anti-Fade Mount (Thermo). Stained sections were imaged using a Leica SPE confocal microscope and are presented at both low and high magnification. Low-magnification images are presented as max projections (∼60 μm z-stack depth) of composite 3 × 3 tile scans imaged with a 10× air objective. High-magnification images are presented as max projections of (10−12 μm depth) and were taken from within the area presented at low magnification. All images were processed in Fiji (ImageJ open source software).[37]

Porosity and Feature Size Measurement by CARS Microscopy. The ELP gels were characterized in situ by coherent anti-Stokes Raman scattering (CARS) microscopy with an inverted microscope (Nikon Ti2-E with a C2 confocal scanning head and a Nikon CFI Apochromat TIRF 100XC oil immersion objective). The carbon−hydrogen (C−H) vibrations were coherently driven by overlapping two near-infrared laser beams in time and space, generated by a picosecond-pulsed laser system (APE picoEmerald S, 2 ps pulse length, 80 MHz repetition rate, and 10 cm^{-1} bandwidth) composed of a 1031 nm Nd:YAN laser and an optical parametric oscillator (OPO) tunable between 700−960 nm (pumped by the second-harmonic of the 1031 nm laser). The OPO wavelength was set to 791.8 nm to address the protein-specific stretching vibration of CH_3 at 2930 cm^{-1}. The quadratic dependence of the CARS signal on the number density of the probed C−H vibrational group, inherently present in the ELP polymer structure, provides sharp contrast for the polymer-dense regions without the need for external labels or other disruptive sample preparations. In contrast to electron and confocal fluorescence microscopy, CARS assures that the native morphology of the ELP gel in its hydrated condition is characterized. Furthermore, the penetration depth of the near-infrared excitation beams and the automatic confocal sectioning of the third-order CARS process enable probing of the 3D structure deep inside the hydrated ELP gels and at high resolution without concerns for artifacts. The excitation powers at the sample were 13 mW for the 1031 nm beam and 27 mW for the OPO beam, and CARS signals were collected in the forward direction with a photomultiplier tube (Hamamatsu, R6357). Z-stacks (covering a 36.4 μm field of view and a depth of ∼15 μm) were collected with 5.3 μs dwell time, 35 nm pixel size, and 0.25 μm vertical separation between adjacent z-positions. The acquired images were prepared and analyzed in ImageJ (3D visualizations of the gels were subsequently created with the NIS Elements volume viewer). Each slice was normalized through a nonresonant CARS image generated from the coverslip, and the contrasts were equalized throughout each stack. After east shadow correction, the images were bandpass Fourier filtered between 3 and 150 pixels with 5% tolerance of direction and suppression of horizontal stripes. The gel porosity was then extracted by calculating the percentage of pixels with zero value after Otsu thresholding. To evaluate the bead sizes of the ELP polymer-dense regions, a Gaussian blur filter (σ = 3) and Otsu thresholding were applied to the images, followed by the ImageJ plugin for disconnecting particles. The bead sizes were then estimated by fitting the particles with an ellipse.

Statistics. All data are presented as mean ± standard deviation (SD). Replicate count is described in the figure captions, and a complete list of all statistics at all time points is listed in Supporting Information. Statistical significance testing for all data was performed in the GraphPad Prism 7 software package using a one-way ANOVA with significance cutoff of α = 0.05 and posthoc Tukey test. In all figures, significance cutoffs are defined as follows: * $p < 0.05$; ** $p < 0.01$, *** $p < 0.001$, **** $p < 0.0001$.

RESULTS

In this work, we wanted to characterize the ability of ELPs to serve as a synthetic support matrix and guide regenerating

https://dx.doi.org/10.1021/acsbiomaterials.0c01053
ACS Biomater. Sci. Eng. 2021, 7, 4209−4220

axons to their distal targets. To do this, we tested two groups: (1) an ELP-filled silicone conduit and (2) an empty silicone conduit as a control. Our animal cohort was divided into two, sex-matched experimental groups (Table 1). Empty silicone

Table 1. Sprague Dawley Rats in Two Experimental Groups[a]

	animal counts		
	female (♀)	male (♂)	total
ELP	6	6	12
empty	6	7	13

[a]Sprague Dawley Rats (10 weeks old, Mixed ♀/♂) were divided into two experimental groups: ELP-filled silicone conduits (ELP, n = 12) and empty silicone conduits (empty, n = 13).

conduits have been used previously to repair short nerve-gaps (<5 mm) successfully.[47,48] However, longer nerve-gaps (10–15 mm) typically have mixed results with some failing completely to support nerve growth and others supporting partial innervation.[11,49,50] Therefore, for a 10 mm gap bridged by an empty silicone conduit we expected to observe a mix of successful and unsuccessful nerve bridge formations that would serve as an effective means of comparison to ELP-filled conduits.

Our elastin-like protein (ELP) materials have two structural components: a bioactive domain (Bio) and an elastin-like region (Figure 1a). These regions contain amino acid sequences (Figure 1b) with the cell-responsive, fibronectin-derived RGD sequence, which is well-known to permit and enhance neurite extension.[51] In the ELP used here, we have engineered the bioactive domain to specifically contain an extended version of the canonical fibronectin-III sequence that includes both the minimally active RGD peptide in addition to several flanking amino acids found natively (extended sequence: TVYAVTGRGDSPASSAA). The inclusion of these flanking amino acids has been suggested to alter the conformational presentation of the RGD ligand and enhance integrin engagement of neuronal cells.[52,53] The elastin-like region is based on the canonical human elastin sequence $(VPGXG)_5$, where the "X" residue in the central pentamer repeat was chosen to be lysine, which has a primary amine side chain. Amino acid analysis of our full protein along with representative proton nuclear magnetic resonance (H1 NMR) and Fourier-transform infrared spectroscopy (FTIR) spectra have been included in Supporting Information for reference (Figure S1). The presence of this central lysine group allows for noncytotoxic cross-linking into a hydrogel via reaction with the amine-reactive cross-linker tetrakis(hydroxymethyl)-phosphonium chloride (THPC).[54] Our previous work with these materials demonstrated that *in vitro* neurite extension from chick DRG cultures was significantly enhanced in ELP hydrogels with (1) higher cell-adhesive RGD peptide sequence concentration (3.1 mM) compared to hydrogels with lower RGD peptide concentration (0 and 1.5 mM) and additionally (2) in hydrogels that were more compliant (shear modulus, G = 0.5–1.0 kPa) compared to stiffer hydrogels (1.5–2.5 kPa).[33]

On the basis of these previous results, we sought to test an ELP hydrogel in vivo that matched this higher concentration RGD and lower mechanical stiffness. First, the hydrogels were cross-linked with THPC for 30 min at room temperature (23 °C). Gelation was indicated by the crossover point (storage modulus greater than loss modulus: $G' > G''$) which was

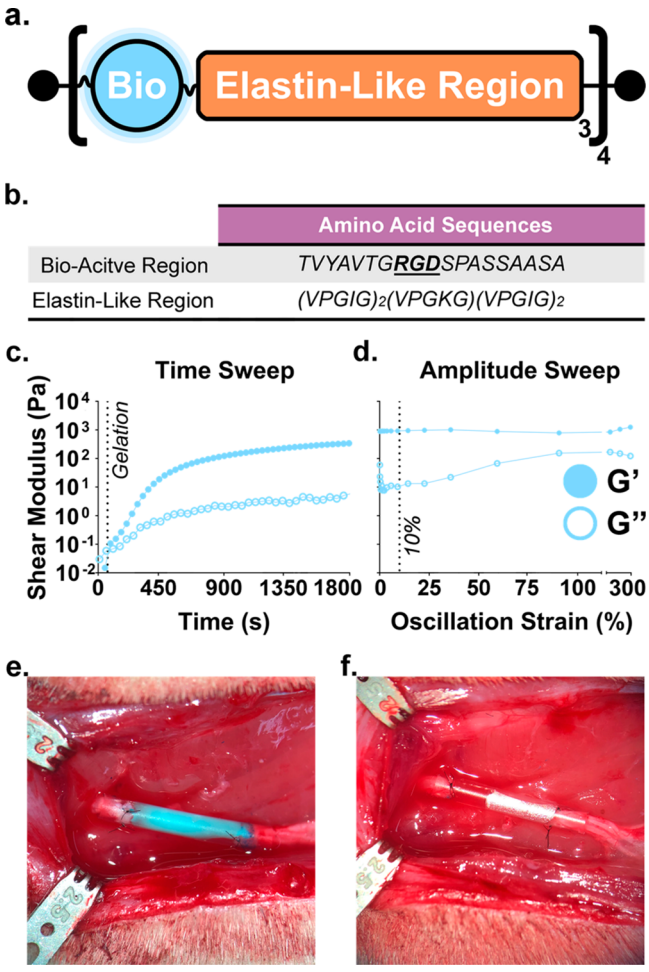

Figure 1. ELP schematic, mechanics, and implant model. (a) Schematic of our elastin-like protein (ELP). (b) Amino acid sequences of selected regions of our ELP. (c) After mixing ELP and amine-reactive tetrakis(hydroxymethyl)phosphonium chloride (THPC), gelation begins (indicated by the crossover-point: $G' > G''$) at approximately 60 s and reaches a plateau after 30 min at room temperature (plateau storage modulus, G': ~ 500 Pa). (d) Warming ELP hydrogels to 37 °C and incubating for 15 min led to the formation of robust gels of approximately ~900 Pa (918.98 ± 140.60 Pa, n = 4). Hollow silicone conduits can be filled with ELP hydrogels (dyed blue for ease of viewing) (e) or kept empty (f) and implanted at the site of a 10 mm sciatic nerve injury to serve as nerve guidance channels in a rat model.

reached after approximately 60 s. After 30 min of cross-linking, our gels reached a plateau modulus of approximately ~500 Pa (Figure 1c). Following this initial cross-linking step, hydrogels were heated to 37 °C and incubated for 15 min, which induces self-assembly of the elastin-like regions to further stabilize the hydrogel, resulting in a final shear modulus of ~900 Pa (Figure 1d). Using this procedure, we filled the intraluminal space of pretrimmed silicone conduits and found them robust enough to be implanted at the site of a sciatic nerve injury (Figure 1e). Similarly, we validated that we could implant empty silicone conduits (Figure 1f) as a control. A schematic representation of ELP-cross-linking and photographs of the conduit filling process has been included in the Supporting Information (Figure S2).

The PNS, unlike the central nervous system, has a strong potential to regenerate following injury. In the case of crush

https://dx.doi.org/10.1021/acsbiomaterials.0c01053
ACS Biomater. Sci. Eng. 2021, 7, 4209–4220

injuries or minor cuts where nerves are superficially damaged, there is a good chance that patients will have full recovery.[55] In the case of complete transection (neurotmesis), the possibility of recovery is significantly decreased.[55] While the full complexity of the neuro-regenerative process in complete transection injuries is not yet fully understood,[56] a critical step is the formation of what is known as a "nerve bridge" that forms between the proximal and distal nerve stumps.[57] This bridge is important in obtaining successful regeneration because it serves as the substrate over which new axons, guided by chemotactic signals from Schwann cells, travel from the proximal nerve stump to reinnervate their distal targets.[56,58−60] Without this nerve bridge, or a support substrate of some kind, regenerating axons cannot reach their distal targets, and prolonged periods of deinnervation substantially reduce the potential for functional recovery.

After excising our implants, we found that 100% of ELP-filled conduits had evidence of a tissue bridge between the proximal and distal nerve stumps compared to only ∼70% of empty silicone conduits (Figure 2a). Because of the transparency of the silicone tubing, any bridge formation was readily visible in both the ELP-filled (Figure 2b) and empty silicone conduit groups (Figure 2c). Similarly, conduit groups that did not form a tissue bridge were easily identified by the absence of connective tissue between the two nerve ends (Figure 2d). Additionally, comparing tissue sections costained for neurofilament (NF) and myelin basic protein (MBP) of uninjured, contralateral sciatic nerve (Figure 3a) to ELP-regenerated tissue (Figure 3b) and empty silicone regenerated-tissue (Figure 3c), we confirmed that regenerated nerve bridges in both experimental groups contained axonal fibers with positive NF staining, some of which were myelinated (identified by MBP). Myelinated axons are an important indication of healthy regeneration, as the myelin acts to improve the efficiency of the nerves in successfully transferring electrical signals from the central nervous system to distal muscle groups. Qualitatively, it is interesting to note that we did not observe a difference in the degree of myelination between our experimental groups, supporting the idea that ELP does not impede myelination but may not enhance it at this time point. Additionally, while our ELP hydrogels do not have any kind of engineered guidance built into the conduits to assist in directionality, we saw that the regenerated axons did not appear randomly distributed within the distal portions of the regenerated tissue sections (Figure 3b), similar to tissue regenerated in empty silicone conduits (Figure 3c). In both cases, there was general alignment in these regions with axons spanning from the proximal (left) to distal (right) sides, which is required for innervation to take place. Taken together with our data showing enhanced tissue bridging in ELP conduits (Figure 2a), we conclude that ELP hydrogels support axonal

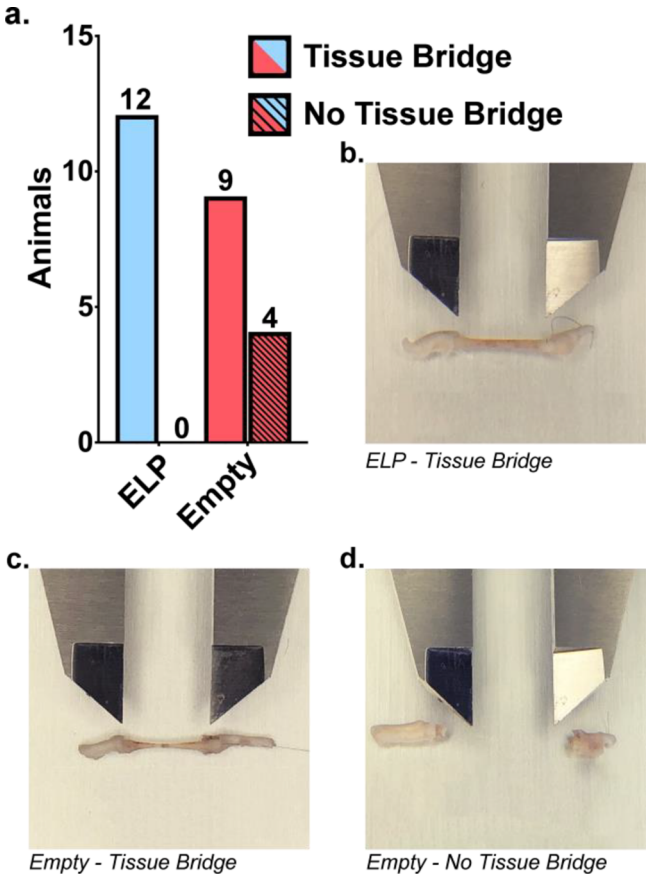

Figure 2. Tissue bridge formation. (a) At 6 weeks, we found that 100% (12/12) of animals treated with an ELP-filled conduit had evidence of a regenerated tissue bridge between the proximal and distal ends, whereas only ∼70% (9/13) of animals in the empty silicone conduit group did. Examples of isolated gross tissue samples from the (b) ELP-filled and (c) empty silicone conduit groups show a clear "bridge" between the proximal (right) and distal (left) sections of the nerve. (d) In contrast, empty silicone conduits that failed to regenerate tissue across the injury gap were clearly evidenced by the absence of any outgrowth.

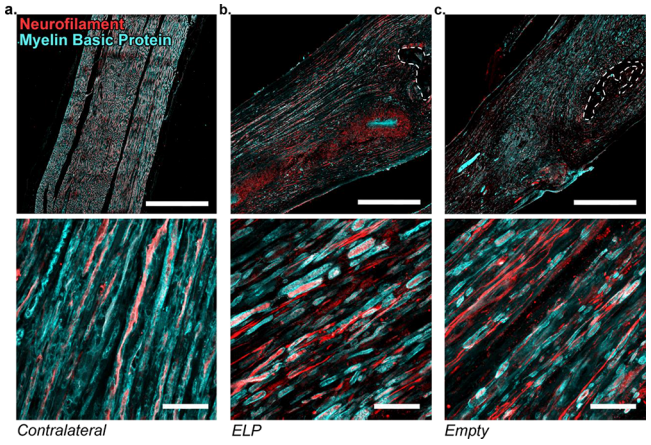

Figure 3. Axonal regeneration and myelination. Representative low-magnification (top) and high-magnification (bottom) immunocytochemistry images of a (a) contralateral sciatic nerve, and distal portions (last 2 mm) of regenerated-tissue from an (b) ELP-filled conduit and an (c) empty silicone conduit. Tissue sections were stained with antineurofilament (NF; red) and antimyelin basic protein (MBP; cyan) antibodies. Healthy myelinated axonal fibers with MBP + regions surrounding NF+ regions in contralateral slices have been included as a positive control and for reference. In the low-magnification images of both experimental groups, alignment of regenerated axons can generally be observed spanning from the proximal side (left) to the distal side (right) of the images. The location of a void left behind by a suturing scar has been denoted by a dottedline. Looking at higher-magnification images from within these same regions, tissue within both the ELP-filled and empty silicone conduits demonstrate evidence of myelinated axonal fibers. Scale bar in low magnification images represents 500 μm; scale bar in high magnification represents 25 μm.

https://dx.doi.org/10.1021/acsbiomaterials.0c01053
ACS Biomater. Sci. Eng. 2021, 7, 4209−4220

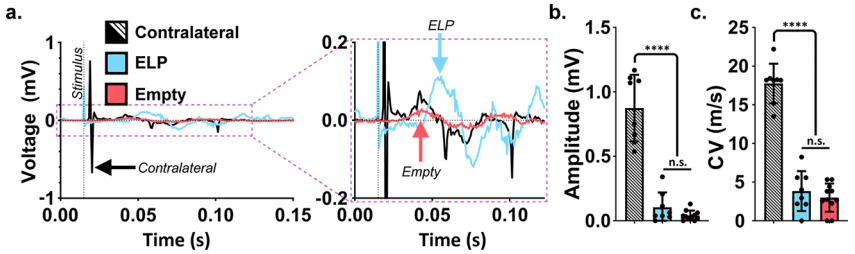

Figure 4. Electrophysiology. (a) Representative CMAP curves at 6 weeks. The stimulus is labeled for reference. Right: Zoomed-in version for ease of viewing the results from ELP-filled and empty conduits. Arrows indicate the first resulting positive peak from which the amplitude and conduction velocity (CV) were calculated. (b) Amplitude and (c) CV between the ELP (n = 8) and empty silicone conduit groups (n = 11) have no significant (n.s.) differences in either measurement. As expected, the corresponding contralateral amplitude (0.87 ± 0.25 mv (n = 8)) and CV (17.74 ± 2.56 m/s, (n = 8) were significantly larger (****, p < 0.0001) than both experimental groups. All data are presented as the mean and standard deviation (SD). Black circles represent individual animal measurements. Statistical test: one-way ANOVA α = 0.05, posthoc Tukey test.

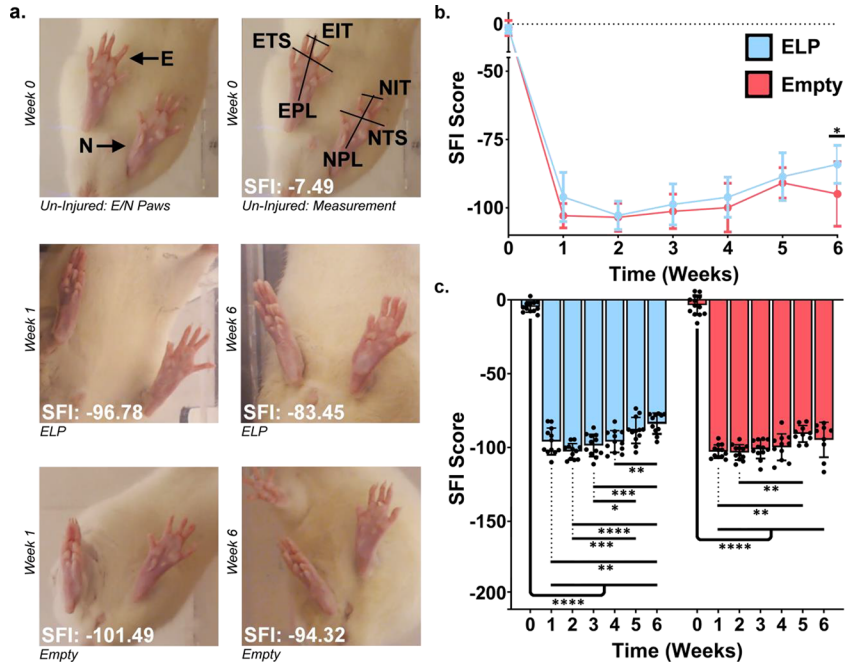

Figure 5. Sciatic functional index. (a) The SFI score was calculated by manually measuring the plantar length (PL), toe spread (TS), and intermediary toe spread (ITS) from the experimental (E) and contralateral (N) paws from screenshots extracted from a video recording of each subject at weekly time points; representative pawprints of the average SFI for each group are shown (see Materials and Methods for detailed description). (b) By week 6, we observed a significant difference (*, p < 0.05) between the ELP-filled conduit (−83.74 ± 6.98, n = 11) and the empty silicone conduit group (−94.92 ± 11.81, n = 9) showing that animals with an ELP-filled conduit had a greater degree of motor nerve function than those with an empty silicone conduit. All data are presented as the mean and standard deviation (SD). Black circles represent individual animal measurements. Statistical test: one-way ANOVA α = 0.05, posthoc Tukey test.

regeneration and myelination *in vivo* and improve the probability of extending axons reaching their distal target.

While guiding axonal fibers from the proximal stump across the length of a nerve gap is a critical first step in regeneration, successful functional recovery is only possible when axons reinnervate their distal targets. Experimentally, the extent of motor neuron innervation and overall motor neuron health are commonly assessed by analyzing the compound muscle action potential (CMAP) measured in distal muscle groups following direct stimulation of the target nerve.[44] Here, we measured CMAP in the muscles of the anterior experimental paw (hind right) following direct stimulation of the sciatic nerve approximately ∼3 mm proximal to the nerve implant. From these stimulations, we collected raw CMAP data (Figure 4a; individual representative peaks available in Figure S3) and tabulated the resulting amplitude and conduction velocities (CV). As expected, CMAP values were zero (no signal detected) for individuals displaying no tissue bridge formation, whereas a robust signal was found on the contralateral side which was used here as a control. Within our experimental groups, there was no statistically significant difference between the two implant groups in either the amplitude (Figure 4b) or CV (Figure 4c), although we note that the ELP-filled conduit group did have overall higher values (complete data set available in Table S1).

To quantify how this measured innervation translated to functional recovery, we measured the sciatic functional index (SFI) from video recordings of our animals (Figure 5a) at weekly time points using empirical equations previously reported by Bain et al.[36] By week 6, animals that had received an ELP-filled conduit had a significantly higher SFI score than animals that received an empty silicone conduit (*, p < 0.05),

https://dx.doi.org/10.1021/acsbiomaterials.0c01053
ACS Biomater. Sci. Eng. 2021, 7, 4209−4220

suggesting a greater degree of functional control in ELP-treated animals (Figure 5b). The full SFI data set available is presented in Table S2 and a normalized version of the SFI data has also been reported in Figure S4 for reference. Additionally, our measured SFI index for ELP-conduits (mean: −83.45) is similar to SFI values measured for autografts used in identical 10 mm injury models from the literature (approximately −85) suggesting similar degrees of recovery at this time point.[61,62] Furthermore, to evaluate relative recovery over time, we looked at the change in SFI over the course of our experiment within both treatment groups and found that there was significant recovery between weeks 1 and 6 for the ELP-filled conduit group ($p < 0.01$, Figure 5c) but not for the empty silicone conduit group (Figure 5d).

Along with SFI, we measured sensory recovery using two sensory tests. In this study, we opted to use a modified version of the von Frey fiber test in addition to the hot plate test because there is evidence that they may give the most easily distinguishable pain response in rats following sciatic nerve injury.[63] As is common for sensory tests, there was a high degree of individual animal variability, presumably resulting from nonuniform sensitivity distribution in the paws and subject-specific, pain-response thresholds.[64,65] Collectively, this prevented us from drawing meaningful conclusions regarding sensory recovery, but we have included this information in Supporting Information for reference (Figure S5 and Figure S6). Additionally, we measured muscle atrophy by looking at the wet muscle mass of the tibialis anterior (TA) and gastrocnemius (GT) muscles relative to the corresponding contralateral muscles. As expected for this early 6 week time point, we did not see any significant differences between the ELP-filled and empty silicone conduit groups (Figure S7).

DISCUSSION

The goal of this study was to evaluate the potential use of a protein-engineered hydrogel as an intraluminal filler in an off-the-shelf-available NGC. Taken together, our data suggest that ELP hydrogels can be used to enhance the probability of recovery *in vivo* compared to empty silicone conduits. The use of a support matrix inside a hollow tube has been shown previously to help improve the likelihood of nerves bridging a transection injury.[66,67] A variety of different naturally derived materials have previously been used as luminal fillers to promote peripheral nerve repair in guidance conduits.[12−17] For example, Chen et al. used a similar experimental design as the one presented here, and they observed that 100% of silicone conduits filled with collagen, laminin, and fibronectin mixtures regenerated nerves across a 10 mm gap compared to only 60% of empty silicone conduit groups at six-weeks post implantation.[67] Our results using the protein-engineered ELP hydrogels show similar degrees of axonal support and marked improvement over empty silicone conduits. Compared to naturally produced extracellular matrix proteins, recombinantly produced ELP proteins may be more cost-effective, more reproducible, and enable a greater degree of customization due to the exact specification of the entire amino acid sequence.

Protein-engineered, ELP biomaterials have been designed with a broad array of cell-adhesive, self-assembly, biodegradation, and mechanical properties.[33,68−70] Here we selected an ELP formulation that was similar to the best-performing hydrogel in our previous *in vitro* study in order to perform a baseline study of *in vivo* feasibility.[33] This study represents a foundational first step in validating ELP hydrogels as viable candidates for synthetic NGC. In the future, the tunability of the ELP system would lend itself well to an optimization study to identify the exact hydrogel properties that most promote nerve regeneration. Previously, our lab has extensively characterized many properties of these ELP hydrogels that may be relevant to nerve regeneration. We have used coherent anti-Stokes Raman scattering (CARS) microscopy to characterize the microstructure of these hydrogels, which form an interconnected network of polymer-rich and polymer-lean regions due to the hydrophobic character of the elastin-like sequence.[32,71] For the specific ELP hydrogels used here, we quantified an approximate overall porosity of 54.1% (Figure S8). During cross-linking, ELP self-assembles into a bead-string structure where, using an ellipsis fit, we approximated a major and minor axis length of 0.97 ± 0.02 μm and 0.64 ± 0.01 μm, respectively (Figure S8). Because of this large porosity, we have previously shown that diffusivity is independent of cross-linking density for ELP gels with a diffusivity range from 20 to 80 $\mu m^2/s$ for solutes with a radius of hydration from 3 to 10.5 nm, respectively.[32] Finally, we have also previously shown that our gels can undergo cell-induced degradation through the proteolytic action of MMPs.[32,72] Neurite extension is known to be heavily influenced by the complex relationship between many matrix properties: porosity, degradability, cell-adhesive ligand concentration, and the relative permeability of nutrients being among them.[73−76] Consequently, when designing matrix materials, there is likely an optimum space between all of these factors that is system dependent and should be evaluated for each unique material.

As one example of a particularly important material property for future optimization, hydrogel mechanics is known to significantly influence cell behavior.[77] Because of this influence, it has often been suggested that biomaterials should be designed to have a stiffness that matches the tissue they are intending to replace or regenerate.[78] This can be challenging from a design perspective because the mechanical testing of tissue reported within the literature is highly variable. Peripheral nerve tissue in particular has not been as well characterized,[78] with a wide range of possible stiffnesses (0.5−54 kPa) having been reported.[79−81] The ELP hydrogel used here is at the lower end of this range (∼1.0 kPa) and was selected because reports by us and others have demonstrated that three-dimensional neurite outgrowth *in vitro* is significantly improved in decreasingly softer matrices.[33,82] However, future studies should explicitly explore if trends observed *in vitro* are also observed during *in vivo* regeneration to demonstrate robustness of these predictions and better direct future materials' design. Beyond hydrogel mechanics, additional complexity could be explored by designing ELPs that contain different cell-adhesive ligands to mimic the native regenerative microenvironment.

In addition to broadening the design space of the ELP hydrogel, future studies should evaluate recovery at longer time points and with greater challenges (e.g., longer nerve gaps). In particular, validating nerve repair with a fully synthetic graft for a 2−3 cm injury over the course of several months to a year would help to fully evaluate their potential, as these lengths and time-points are more clinically relevant.[83] The animal model selected here (a 10 mm gap over 6 weeks) was selected to be consistent with other previously published work.[66,67] While this shorter time-point is ideal for tissue-bridging studies, functional regeneration in PNI models, even with the

https://dx.doi.org/10.1021/acsbiomaterials.0c01053
ACS Biomater. Sci. Eng. 2021, 7, 4209−4220

"gold standard" autograft, can take upward of months to a year to begin approaching preinjury levels (SFI: −70 to −60).[61,62,84] Consistent with these previous reports, we observed that peripheral nerve function values were all much lower at 6 weeks than the preinjured state (Figures 3, S3, and S4). Within our behavioral data, we measured a drop between weeks 1 and 2 in SFI for both groups (Figure 3). This trend in decreasing SFI score has been observed in other studies[85] but is not always the case.[18] Importantly, it does not appear to be related to injury type (crush or transection). One study specifically looking at SFI measurement variability reported that the first 2 weeks are highly susceptible to inconsistency between reported values and suggested this is due to difficulty in reliably measuring foot dimensions following surgery.[85] Nevertheless, significant differences in SFI between the ELP-filled and empty conduits had emerged by the six-week time point used here, and these results support the future study of extended time points.

Given the success of these initial results and the demonstrated tunability of this hydrogel system, ELPs could be used to present an optimized, off-the-shelf alternative to promote peripheral nerve regeneration.

CONCLUSIONS

Our data shows that ELP hydrogels offer a beneficial support matrix for regenerating axons *in vivo* compared to empty silicone constructs. In this work, we compared two groups, silicone conduits filled with ELP intraluminal filler and an empty silicone conduit in treating a 10 mm sciatic nerve injury in 10 week old Sprague-Dawley rats (ELP, n = 12; empty, n = 13). At 6 weeks, ELP-filled conduits had a greater degree of tissue bridge formation (100%) between the proximal and distal nerve stumps as compared to empty silicone conduits (70%). Furthermore, we showed that both groups had immunocytochemical evidence of myelinated axons and CMAP evidence of distal muscle innervation, both of which are critical in healthy, functional recovery. In parallel with this, we measured functional recovery with weekly sciatic functional index (SFI) tests and saw that animals in the ELP-filled conduit group had a significantly improved SFI score, indicating that the ELP therapy resulted in greater locomotor function. Given these results, our future studies with this ELP hydrogel material will evaluate longer time points and larger nerve-injury gaps to further validate and optimize this system as an off-the-shelf alternative to current therapies.

ASSOCIATED CONTENT

Supporting Information

The Supporting Information is available free of charge at https://pubs.acs.org/doi/10.1021/acsbiomaterials.0c01053.

Figure S1: Elastin-Like Protein Amino Acid Analysis and Representative Spectra Figure S2: Elastin-Like Protein Crosslinking Schematic and Conduit Fabrication Photographs Figure S3: Representative Individual Electrophysiology Curves Table S1: Electrophysiology Data Summary Table S2: Sciatic Functional Index Data Summary Figure S4: Normalized Sciatic Functional Index Data Figure S5: Needle Poke Test: Methods, plots, and data summary Figure S6: Hot-Plate Test: Methods, Plots, and Data Summary Figure S7: Wet Muscle Mass: Methods, Plots, and Data Summary Figure S8: Coherent anti-Stokes Raman Spectroscopy of Elastin-Like Protein Hydrogel (PDF)

AUTHOR INFORMATION

Corresponding Author

Sarah C. Heilshorn − *Department of Materials Science and Engineering, Stanford University, Stanford, California 94305, United States;* orcid.org/0000-0002-9801-6304; Email: heilshorn@stanford.edu

Authors

Riley A. Suhar − *Department of Materials Science and Engineering, Stanford University, Stanford, California 94305, United States*

Laura M. Marquardt − *Department of Materials Science and Engineering, Stanford University, Stanford, California 94305, United States; Department of Neurosurgery, Stanford University School of Medicine, Stanford, California 94305, United States*

Shang Song − *Department of Neurology and Neurological Sciences, Stanford University School of Medicine, Stanford, California 94305, United States*

Hana Buabbas − *Department of Biology, Stanford University, Stanford, California 94305, United States*

Vanessa M. Doulames − *Department of Neurosurgery, Stanford University School of Medicine, Stanford, California 94305, United States*

Patrik K. Johansson − *Department of Materials Science and Engineering, Stanford University, Stanford, California 94305, United States*

Katarina C. Klett − *Program in Stem Cell Biology and Regenerative Medicine, Stanford University School of Medicine, Stanford, California 94305, United States*

Ruby E. Dewi − *Department of Materials Science and Engineering, Stanford University, Stanford, California 94305, United States*

Annika M. K. Enejder − *Department of Materials Science and Engineering, Stanford University, Stanford, California 94305, United States;* orcid.org/0000-0003-2000-1353

Giles W. Plant − *Department of Neurosurgery, Stanford University School of Medicine, Stanford, California 94305, United States*

Paul M. George − *Department of Neurology and Neurological Sciences and Stanford Stroke Center, Stanford University School of Medicine, Stanford, California 94305, United States*

Complete contact information is available at: https://pubs.acs.org/10.1021/acsbiomaterials.0c01053

Notes

The authors declare no competing financial interest.

ACKNOWLEDGMENTS

We acknowledge C. Madl for helpful discussions on fabricating nerve guidance conduits and experimental design; your support and mentorship were invaluable. We acknowledge conversations with B. LeSavage on data interpretation, advice for statistical tests, and data presentation. We thank K. Casey and D. Wu from the Stanford Animal Histology Services for help with preparation of histological specimens. Additionally, we would like to thank C. Plant for taking the time to help in editing and reviewing this manuscript. This work was supported by the National Institutes of Health (NIH) Training Grant in Biotechnology (T32-GM008412) to R.A.S.; Training

Grant in Stem Cell Biology and Regenerative Medicine (T32-GM119995) to K.C.K.; Grants R21-NS114549 and R01-EB027171 to S.C.H.; R01-EB027666 to G.W.P.; F32-HD098808 to S.S.; K08-NS089976 to P.G.; the Alliance for Regenerative Rehabilitation Research and Training (AR3T) supported by NIH P2C-HD086843 to P.G. and S.C.H.; the Stanford Lieberman Fellowship (R.A.S.); the Wu Tsai Neurosciences Institute NeuroTranslate Award (S.C.H. and P.M.G.); the National Science Foundation (1808415 to S.C.H.), the Wu Tsai Neurosciences Institute Interdisciplinary Postdoctoral Fellowship (L.M.M.); Department of Defense (SCRIP SC170085 to G.W.P.); and Wings for Life (WFL-US-020/14 to G.W.P.). Part of this work was performed at the Stanford Nano Shared Facilities (SNSF), supported by the National Science Foundation under award ECCS-1542152.

REFERENCES

(1) Frostick, S. P.; Yin, Q.; Kemp, G. J. Schwann Cells, Neurotrophic Factors, and Peripheral Nerve Regeneration. *Microsurgery* **1998**, *18* (7), 397−405.

(2) Jobe, M. T.; Martinez, S. F. Peripheral Nerve Injuries. In *Campbell's Operative Orthopaedics*; Elsevier: Philadelphia, PA, 2017; pp 3161−3224.

(3) Ruijs, A.; Jaquet, J. B.; Kalmijn, S.; Giele, H.; Hovius, S. Median and Ulnar Nerve Injuries: A Meta-Analysis of Predictors of Motor and Sensory Recovery after Modern Microsurgical Nerve Repair. *Plast. Reconstr. Surg.* **2005**, *116* (2), 484−494.

(4) Eser, F.; Aktekin, L. A.; Bodur, H.; Atan, C. Etiological Factors of Traumatic Peripheral Nerve Injuries. *Neurol. India* **2009**, *57* (4), 434−437.

(5) Hood, B.; Levene, H. B.; Levi, A. D. Transplantation of Autologous Schwann Cells for the Repair of Segmental Peripheral Nerve Defects. *Neurosurg. Focus* **2009**, *26* (2), E4.

(6) Schmidt, C. E.; Leach, J. B. Neural Tissue Engineering: Strategies for Repair and Regeneration. *Annu. Rev. Biomed. Eng.* **2003**, *5* (1), 293−347.

(7) Terzis, J. K.; Sun, D. D.; Thanos, P. K. Historical and Basic Science Review: Past, Present, and Future of Nerve Repair. *J. Reconstr. Microsurg.* **1997**, *13* (3), 215−225.

(8) Ray, W. Z.; Mackinnon, S. E. Management of Nerve Gaps: Autografts, Allografts, Nerve Transfers, and End-to-Side Neurorrhaphy. *Exp. Neurol.* **2010**, *223* (1), 77−85.

(9) Karabekmez, F. E.; Duymaz, A.; Moran, S. L. Early Clinical Outcomes with the Use of Decellularized Nerve Allograft for Repair of Sensory Defects Within the Hand. *Hand N. Y. N* **2009**, *4* (3), 245−249.

(10) Daly, W.; Yao, L.; Zeugolis, D.; Windebank, A.; Pandit, A. A Biomaterials Approach to Peripheral Nerve Regeneration: Bridging the Peripheral Nerve Gap and Enhancing Functional Recovery. *J. R. Soc., Interface* **2012**, *9* (67), 202−221.

(11) Williams, L. R.; Longo, F. M.; Powell, H. C.; Lundborg, G.; Varon, S. Spatial-Temporal Progress of Peripheral Nerve Regeneration within a Silicone Chamber: Parameters for a Bioassay. *J. Comp. Neurol.* **1983**, *218* (4), 460−470.

(12) Toba, T.; Nakamura, T.; Shimizu, Y.; Matsumoto, K.; Ohnishi, K.; Fukuda, S.; Yoshitani, M.; Ueda, H.; Hori, Y.; Endo, K. Regeneration of Canine Peroneal Nerve with the Use of a Polyglycolic Acid-Collagen Tube Filled with Laminin-Soaked Collagen Sponge: A Comparative Study of Collagen Sponge and Collagen Fibers as Filling Materials for Nerve Conduits. *J. Biomed. Mater. Res.* **2001**, *58* (6), 622−630.

(13) Lee, D. Y.; Choi, B. H.; Park, J. H.; Zhu, S. J.; Kim, B. Y.; Huh, J. Y.; Lee, S. H.; Jung, J. H.; Kim, S. H. Nerve Regeneration with the Use of a Poly(l-Lactide-Co-Glycolic Acid)-Coated Collagen Tube Filled with Collagen Gel. *J. Cranio-Maxillo-fac. Surg. Off. Publ. Eur. Assoc. Cranio-Maxillo-fac. Surg.* **2006**, *34* (1), 50−56.

(14) Sierpinski, P.; Garrett, J.; Ma, J.; Apel, P.; Klorig, D.; Smith, T.; Koman, L. A.; Atala, A.; Van Dyke, M. The Use of Keratin Biomaterials Derived from Human Hair for the Promotion of Rapid Regeneration of Peripheral Nerves. *Biomaterials* **2008**, *29* (1), 118−128.

(15) Wood, M. D.; Gordon, T.; Kim, H.; Szynkaruk, M.; Phua, P.; Lafontaine, C.; Kemp, S. W.; Shoichet, M. S.; Borschel, G. H. Fibrin Gels Containing GDNF Microspheres Increase Axonal Regeneration after Delayed Peripheral Nerve Repair. *Regener. Med.* **2013**, *8* (1), 27−37.

(16) Scott, R.; Marquardt, L.; Willits, R. K. Characterization of Poly(Ethylene Glycol) Gels with Added Collagen for Neural Tissue Engineering. *J. Biomed. Mater. Res., Part A* **2010**, *93* (3), 817−823.

(17) Choi, J.; Kim, J. H.; Jang, J. W.; Kim, H. J.; Choi, S. H.; Kwon, S. W. Decellularized Sciatic Nerve Matrix as a Biodegradable Conduit for Peripheral Nerve Regeneration. *Neural Regener. Res.* **2018**, *13* (10), 1796−1803.

(18) Kokai, L. E.; Bourbeau, D.; Weber, D.; McAtee, J.; Marra, K. G. Sustained Growth Factor Delivery Promotes Axonal Regeneration in Long Gap Peripheral Nerve Repair. *Tissue Eng., Part A* **2011**, *17* (9−10), 1263−1275.

(19) Mohanna, P. N.; Young, R. C.; Wiberg, M.; Terenghi, G. A Composite Poly-Hydroxybutyrate-Glial Growth Factor Conduit for Long Nerve Gap Repairs. *J. Anat.* **2003**, *203* (6), 553−565.

(20) Hsu, S. H.; Ni, H. C. Fabrication of the Microgrooved/Microporous Polylactide Substrates as Peripheral Nerve Conduits and in Vivo Evaluation. *Tissue Eng., Part A* **2009**, *15* (6), 1381−1390.

(21) Oh, S. H.; Kim, J. H.; Song, K. S.; Jeon, B. H.; Yoon, J. H.; Seo, T. B.; Namgung, U.; Lee, I. W.; Lee, J. H. Peripheral Nerve Regeneration within an Asymmetrically Porous PLGA/Pluronic F127 Nerve Guide Conduit. *Biomaterials* **2008**, *29* (11), 1601−1609.

(22) Li, A.; Hokugo, A.; Yalom, A.; Berns, E. J.; Stephanopoulos, N.; McClendon, M. T.; Segovia, L. A.; Spigelman, I.; Stupp, S. I.; Jarrahy, R. A Bioengineered Peripheral Nerve Construct Using Aligned Peptide Amphiphile Nanofibers. *Biomaterials* **2014**, *35* (31), 8780−8790.

(23) Tirrell, D. A. Artificial Polypeptides. In *Encyclopedia of Materials: Science and Technology*; Buschow, K. H. J., Cahn, R. W., Flemings, M. C., Ilschner, B., Kramer, E. J., Mahajan, S., Veyssière, P., Eds.; Elsevier: Oxford, 2001; pp 347−355.

(24) Gomes, S.; Leonor, I. B.; Mano, J. F.; Reis, R. L.; Kaplan, D. L. Natural and Genetically Engineered Proteins for Tissue Engineering. *Prog. Polym. Sci.* **2012**, *37* (1), 1−17.

(25) Jones, D. S.; Silverman, A. P.; Cochran, J. R. Developing Therapeutic Proteins by Engineering Ligand−Receptor Interactions. *Trends Biotechnol.* **2008**, *26* (9), 498−505.

(26) Rucker, R. B.; Tinker, D. Structure and Metabolism of Arterial Elastin. *Int. Rev. Exp. Pathol.* **1977**, *17*, 1−47.

(27) Lefevre, M.; Rucker, R. B. Aorta Elastin Turnover in Normal and Hypercholesterolemic Japanese Quail. *Biochim. Biophys. Acta, Gen. Subj.* **1980**, *630* (4), 519−529.

(28) Shapiro, S. D.; Endicott, S. K.; Province, M. A.; Pierce, J. A.; Campbell, E. J. Marked Longevity of Human Lung Parenchymal Elastic Fibers Deduced from Prevalence of D-Aspartate and Nuclear Weapons-Related Radiocarbon. *J. Clin. Invest.* **1991**, *87* (5), 1828−1834.

(29) Straley, K. S.; Heilshorn, S. C. Independent Tuning of Multiple Biomaterial Properties Using Protein Engineering. *Soft Matter* **2009**, *5* (1), 114−124.

(30) Romano, N. H.; Madl, C. M.; Heilshorn, S. C. Matrix RGD Ligand Density and L1CAM-Mediated Schwann Cell Interactions Synergistically Enhance Neurite Outgrowth. *Acta Biomater.* **2015**, *11*, 48−57.

(31) LeSavage, B. L.; Suhar, N. A.; Madl, C. M.; Heilshorn, S. C. Production of Elastin-like Protein Hydrogels for Encapsulation and Immunostaining of Cells in 3D. *J. Visualized Exp.* **2018**, *135*, e57739.

(32) Madl, C. M.; LeSavage, B. L.; Dewi, R. E.; Dinh, C. B.; Stowers, R. S.; Khariton, M.; Lampe, K. J.; Nguyen, D.; Chaudhuri, O.; Enejder, A.; Heilshorn, S. C. Maintenance of Neural Progenitor Cell

https://dx.doi.org/10.1021/acsbiomaterials.0c01053
ACS Biomater. Sci. Eng. 2021, 7, 4209−4220

Stemness in 3D Hydrogels Requires Matrix Remodelling. *Nat. Mater.* **2017**, *16* (12), 1233−1242.
(33) Lampe, K. J.; Antaris, A. L.; Heilshorn, S. C. Design of Three-Dimensional Engineered Protein Hydrogels for Tailored Control of Neurite Growth. *Acta Biomater.* **2013**, *9* (3), 5590−5599.
(34) Sinclair, S. M.; Bhattacharyya, J.; McDaniel, J. R.; Gooden, D. M.; Gopalaswamy, R.; Chilkoti, A.; Setton, L. A. A Genetically Engineered Thermally Responsive Sustained Release Curcumin Depot to Treat Neuroinflammation. *J. Controlled Release* **2013**, *171* (1), 38−47.
(35) Geuna, S. The Sciatic Nerve Injury Model in Pre-Clinical Research. *J. Neurosci. Methods* **2015**, *243*, 39−46.
(36) Bain, J. R.; Mackinnon, S. E.; Hunter, D. A. Functional Evaluation of Complete Sciatic, Peroneal, and Posterior Tibial Nerve Lesions in the Rat. *Plast. Reconstr. Surg.* **1989**, *83* (1), 129−138.
(37) Schindelin, J.; Arganda-Carreras, I.; Frise, E.; Kaynig, V.; Longair, M.; Pietzsch, T.; Preibisch, S.; Rueden, C.; Saalfeld, S.; Schmid, B.; Tinevez, J.-Y.; White, D. J.; Hartenstein, V.; Eliceiri, K.; Tomancak, P.; Cardona, A. Fiji: An Open-Source Platform for Biological-Image Analysis. *Nat. Methods* **2012**, *9* (7), 676−682.
(38) Varejão, A. S. P.; Melo-Pinto, P.; Meek, M. F.; Filipe, V. M.; Bulas-Cruz, J. Methods for the Experimental Functional Assessment of Rat Sciatic Nerve Regeneration. *Neurol. Res.* **2004**, *26* (2), 186−194.
(39) Zellem, R. T.; Miller, D. W.; Kenning, J. A.; Hoenig, E. M.; Buchheit, W. A. Experimental Peripheral Nerve Repair: Environmental Control Directed at the Cellular Level. *Microsurgery* **1989**, *10* (4), 290−301.
(40) Weber, R. A.; Proctor, W. H.; Warner, M. R.; Verheyden, C. N. Autotomy and the Sciatic Functional Index. *Microsurgery* **1993**, *14* (5), 323−327.
(41) Oh, S. S.; Hayes, J. M.; Sims-Robinson, C.; Sullivan, K. A.; Feldman, E. L. The Effects of Anesthesia on Measures of Nerve Conduction Velocity in Male C57Bl6/J Mice. *Neurosci. Lett.* **2010**, *483* (2), 127−131.
(42) Zotova, E. G.; Arezzo, J. C. Non-invasive evaluation of nerve conduction in small diameter fibers in the rat. *Physiol. J.* **2013**, *2013*. 1.
(43) Mokarram, N.; Dymanus, K.; Srinivasan, A.; Lyon, J. G.; Tipton, J.; Chu, J.; English, A. W.; Bellamkonda, R. V. Immunoengineering Nerve Repair. *Proc. Natl. Acad. Sci. U. S. A.* **2017**, *114* (26), E5077−E5084.
(44) Hort-Legrand, C.; Noah, L.; Mériguet, E.; Mésangeau, D. Motor and Sensory Nerve Conduction Velocities in Yucatan Minipigs. *Lab. Anim.* **2006**, *40* (1), 53−57.
(45) Shi, S. R.; Chaiwun, B.; Young, L.; Cote, R. J.; Taylor, C. R. Antigen Retrieval Technique Utilizing Citrate Buffer or Urea Solution for Immunohistochemical Demonstration of Androgen Receptor in Formalin-Fixed Paraffin Sections. *J. Histochem. Cytochem.* **1993**, *41* (11), 1599−1604.
(46) Brown, R. W.; Chirala, R. Utility of Microwave-Citrate Antigen Retrieval in Diagnostic Immunohistochemistry. *Mod. Pathol. Off. J. U. S. Can. Acad. Pathol. Inc* **1995**, *8* (5), 515−520.
(47) Kemp, S. W. P.; Syed, S.; Walsh, S. K.; Zochodne, D. W.; Midha, R. Collagen Nerve Conduits Promote Enhanced Axonal Regeneration, Schwann Cell Association, and Neovascularization Compared to Silicone Conduits. *Tissue Eng., Part A* **2009**, *15* (8), 1975−1988.
(48) Lundborg, G.; Rosén, B.; Dahlin, L.; Holmberg, J.; Rosén, I. Tubular Repair of the Median or Ulnar Nerve in the Human Forearm: A 5-Year Follow-Up. *J. Hand Surg. Br. Eur. Vol.* **2004**, *29* (2), 100−107.
(49) Francel, P. C.; Francel, T. J.; Mackinnon, S. E.; Hertl, C. Enhancing Nerve Regeneration across a Silicone Tube Conduit by Using Interposed Short-Segment Nerve Grafts. *J. Neurosurg.* **1997**, *87* (6), 887−892.
(50) Lundborg, G.; Dahlin, L. B.; Danielsen, N.; Gelberman, R. H.; Longo, F. M.; Powell, H. C.; Varon, S. Nerve Regeneration in Silicone Chambers: Influence of Gap Length and of Distal Stump Components. *Exp. Neurol.* **1982**, *76* (2), 361−375.
(51) Schense, J. C.; Hubbell, J. A. Three-Dimensional Migration of Neurites Is Mediated by Adhesion Site Density and Affinity. *J. Biol. Chem.* **2000**, *275* (10), 6813−6818.
(52) Meiners, S.; Mercado, M. L. T. Functional Peptide Sequences Derived from Extracellular Matrix Glycoproteins and Their Receptors: Strategies to Improve Neuronal Regeneration. *Mol. Neurobiol.* **2003**, *27* (2), 177−196.
(53) Morimatsu, M.; Mekhdjian, A. H.; Adhikari, A. S.; Dunn, A. R. Molecular Tension Sensors Report Forces Generated by Single Integrin Molecules in Living Cells. *Nano Lett.* **2013**, *13* (9), 3985−3989.
(54) Chung, C.; Lampe, K. J.; Heilshorn, S. C. Tetrakis-(Hydroxymethyl) Phosphonium Chloride as a Covalent Cross-Linking Agent for Cell Encapsulation within Protein-Based Hydrogels. *Biomacromolecules* **2012**, *13* (12), 3912−3916.
(55) Nguyen, Q. T.; Sanes, J. R.; Lichtman, J. W. Pre-Existing Pathways Promote Precise Projection Patterns. *Nat. Neurosci.* **2002**, *5* (9), 861−867.
(56) Parrinello, S.; Napoli, I.; Ribeiro, S.; Digby, P. W.; Fedorova, M.; Parkinson, D. B.; Doddrell, R. D. S.; Nakayama, M.; Adams, R. H.; Lloyd, A. C. EphB Signaling Directs Peripheral Nerve Regeneration through Sox2-Dependent Schwann Cell Sorting. *Cell* **2010**, *143* (1), 145−155.
(57) Sulaiman, W.; Gordon, T. Neurobiology of Peripheral Nerve Injury, Regeneration, and Functional Recovery: From Bench Top Research to Bedside Application. *Ochsner J.* **2013**, *13* (1), 100−108.
(58) Cattin, A.-L.; Burden, J. J.; Van Emmenis, L.; Mackenzie, F. E.; Hoving, J. J. A.; Garcia Calavia, N.; Guo, Y.; McLaughlin, M.; Rosenberg, L. H.; Quereda, V.; Jamecna, D.; Napoli, I.; Parrinello, S.; Enver, T.; Ruhrberg, C.; Lloyd, A. C. Macrophage-Induced Blood Vessels Guide Schwann Cell-Mediated Regeneration of Peripheral Nerves. *Cell* **2015**, *162* (5), 1127−1139.
(59) Dun, X.; Parkinson, D. B. Visualizing Peripheral Nerve Regeneration by Whole Mount Staining. *PLoS One* **2015**, *10* (3), e0119168.
(60) Dun, X.; Carr, L.; Woodley, P. K.; Barry, R. W.; Drake, L. K.; Mindos, T.; Roberts, S. L.; Lloyd, A. C.; Parkinson, D. B. Macrophage-Derived Slit3 Controls Cell Migration and Axon Pathfinding in the Peripheral Nerve Bridge. *Cell Rep.* **2019**, *26* (6), 1458−1472.
(61) Nagao, R. J.; Lundy, S.; Khaing, Z. Z.; Schmidt, C. E. Functional Characterization of Optimized Acellular Peripheral Nerve Graft in a Rat Sciatic Nerve Injury Model. *Neurol. Res.* **2011**, *33* (6), 600−608.
(62) Kim, J. Y.; Jeon, W. J.; Kim, D. H.; Rhyu, I. J.; Kim, Y. H.; Youn, I.; Park, J. W. An Inside-out Vein Graft Filled with Platelet-Rich Plasma for Repair of a Short Sciatic Nerve Defect in Rats. *Neural Regener. Res.* **2014**, *9* (14), 1351−1357.
(63) Hogan, Q.; Sapunar, D.; Modric-Jednacak, K.; McCallum, J. B. Detection of Neuropathic Pain in a Rat Model of Peripheral Nerve Injury. *Anesthesiology* **2004**, *101* (2), 476−487.
(64) Iggo, A.; Muir, A. R. The Structure and Function of a Slowly Adapting Touch Corpuscle in Hairy Skin. *J. Physiol.* **1969**, *200* (3), 763−796.
(65) Lele, P. P. Relationship between Cutaneous Thermal Thresholds, Skin Temperature and Cross-Sectional Area of the Stimulus. *J. Physiol.* **1954**, *126* (2), 191−205.
(66) Tong, X.; Hirai, K.-I.; Shimada, H.; Mizutani, Y.; Izumi, T.; Toda, N.; Yu, P. Sciatic Nerve Regeneration Navigated by Laminin-Fibronectin Double Coated Biodegradable Collagen Grafts in Rats. *Brain Res.* **1994**, *663* (1), 155−162.
(67) Chen, Y. S.; Hsieh, C. L.; Tsai, C. C.; Chen, T. H.; Cheng, W. C.; Hu, C. L.; Yao, C. H. Peripheral Nerve Regeneration Using Silicone Rubber Chambers Filled with Collagen, Laminin and Fibronectin. *Biomaterials* **2000**, *21* (15), 1541−1547.
(68) Wang, H.; Cai, L.; Paul, A.; Enejder, A.; Heilshorn, S. C. Hybrid Elastin-like Polypeptide-Polyethylene Glycol (ELP-PEG) Hydrogels with Improved Transparency and Independent Control

https://dx.doi.org/10.1021/acsbiomaterials.0c01053
ACS Biomater. Sci. Eng. 2021, 7, 4209−4220

of Matrix Mechanics and Cell Ligand Density. *Biomacromolecules* **2014**, *15* (9), 3421−3428.
(69) Trabbic-Carlson, K.; Setton, L. A.; Chilkoti, A. Swelling and Mechanical Behaviors of Chemically Cross-Linked Hydrogels of Elastin-like Polypeptides. *Biomacromolecules* **2003**, *4* (3), 572−580.
(70) Welsh, E. R.; Tirrell, D. A. Engineering the Extracellular Matrix: A Novel Approach to Polymeric Biomaterials. I. Control of the Physical Properties of Artificial Protein Matrices Designed to Support Adhesion of Vascular Endothelial Cells. *Biomacromolecules* **2000**, *1* (1), 23−30.
(71) Wang, H.; Zhu, D.; Paul, A.; Cai, L.; Enejder, A.; Yang, F.; Heilshorn, S. C. Covalently Adaptable Elastin-Like Protein−Hyaluronic Acid (ELP−HA) Hybrid Hydrogels with Secondary Thermoresponsive Crosslinking for Injectable Stem Cell Delivery. *Adv. Funct. Mater.* **2017**, *27* (28), 1605609.
(72) Chung, C.; Pruitt, B. L.; Heilshorn, S. C. Spontaneous Cardiomyocyte Differentiation of Mouse Embryoid Bodies Regulated by Hydrogel Crosslink Density. *Biomater. Sci.* **2013**, *1* (10), 1082−1090.
(73) Man, A. J.; Davis, H. E.; Itoh, A.; Leach, J. K.; Bannerman, P. Neurite Outgrowth in Fibrin Gels Is Regulated by Substrate Stiffness. *Tissue Eng., Part A* **2011**, *17* (23−24), 2931−2942.
(74) Mahoney, M. J.; Anseth, K. S. Three-Dimensional Growth and Function of Neural Tissue in Degradable Polyethylene Glycol Hydrogels. *Biomaterials* **2006**, *27* (10), 2265−2274.
(75) Gunn, J. W.; Turner, S. D.; Mann, B. K. Adhesive and Mechanical Properties of Hydrogels Influence Neurite Extension. *J. Biomed. Mater. Res.* **2005**, *72A* (1), 91−97.
(76) den Dunnen, W. F.; Stokroos, I.; Blaauw, E. H.; Holwerda, A.; Pennings, A. J.; Robinson, P. H.; Schakenraad, J. M. Light-Microscopic and Electron-Microscopic Evaluation of Short-Term Nerve Regeneration Using a Biodegradable Poly(DL-Lactide-Epsilon-Caprolacton) Nerve Guide. *J. Biomed. Mater. Res.* **1996**, *31* (1), 105−115.
(77) Discher, D. E.; Janmey, P.; Wang, Y.-L. Tissue Cells Feel and Respond to the Stiffness of Their Substrate. *Science* **2005**, *310* (5751), 1139−1143.
(78) Guimarães, C. F.; Gasperini, L.; Marques, A. P.; Reis, R. L. The Stiffness of Living Tissues and Its Implications for Tissue Engineering. *Nat. Rev. Mater.* **2020**, *5* (5), 351−370.
(79) Ma, Z.; Hu, S.; Tan, J. S.; Myer, C.; Njus, N. M.; Xia, Z. In Vitro and in Vivo Mechanical Properties of Human Ulnar and Median Nerves. *J. Biomed. Mater. Res., Part A* **2013**, *101A* (9), 2718−2725.
(80) Rosso, G.; Guck, J. Mechanical Changes of Peripheral Nerve Tissue Microenvironment and Their Structural Basis during Development. *APL Bioeng.* **2019**, *3* (3). 036107.
(81) Borschel, G. H.; Kia, K. F.; Kuzon, W. M.; Dennis, R. G. Mechanical Properties of Acellular Peripheral Nerve. *J. Surg. Res.* **2003**, *114* (2), 133−139.
(82) Balgude, A. P.; Yu, X.; Szymanski, A.; Bellamkonda, R. V. Agarose Gel Stiffness Determines Rate of DRG Neurite Extension in 3D Cultures. *Biomaterials* **2001**, *22* (10), 1077−1084.
(83) Pfister, B. J.; Gordon, T.; Loverde, J. R.; Kochar, A. S.; Mackinnon, S. E.; Cullen, D. K. Biomedical Engineering Strategies for Peripheral Nerve Repair: Surgical Applications, State of the Art, and Future Challenges. *Crit. Rev. Biomed. Eng.* **2011**, *39* (2), 81−124.
(84) Amniattalab, A.; Mohammadi, R. Functional, Histopathological and Immunohistichemical Assessments of Cyclosporine A on Sciatic Nerve Regeneration Using Allografts: A Rat Sciatic Nerve Model. *Bull. Emerg. Trauma* **2017**, *5* (3), 152−159.
(85) Monte-Raso, V. V.; Barbieri, C. H.; Mazzer, N.; Yamasita, A. C.; Barbieri, G. Is the Sciatic Functional Index Always Reliable and Reproducible? *J. Neurosci. Methods* **2008**, *170* (2), 255−261.

https://dx.doi.org/10.1021/acsbiomaterials.0c01053
ACS Biomater. Sci. Eng. 2021, 7, 4209−4220